

Spark Ignition Engine Fuel-to-Air Ratio Control: An Adaptive Control Approach

Yildiray Yildiz, *Student Member, IEEE*, Anuradha M. Annaswamy, *Fellow, IEEE*,
Diana Yanakiev, *Member, IEEE*, Ilya Kolmanovsky, *Fellow, IEEE*

Abstract

This paper presents the control of Spark Ignition (SI) Internal Combustion (IC) engine Fuel-to-Air Ratio (FAR) using an adaptive control method of time-delay systems. The objective is to maintain the in-cylinder FAR at a prescribed set point, determined primarily by the state of the Three-Way Catalyst (TWC), so that the pollutants in the exhaust are removed with the highest efficiency. The FAR controller must also reject disturbances due to canister vapor purge and inaccuracies in air charge estimation and wall-wetting (WW) compensation. Two adaptive controller designs are considered. The first design is based on feedforward adaptation while the second design is based on both feedback and feedforward adaptation incorporating the recently developed Adaptive Posicast Controller (APC). We present both simulation and experimental results demonstrating the performance improvement by employing the APC. We also present the modifications and improvements to the APC structure which were developed during the course of experimentation to solve specific implementation problems.

Index Terms

Road vehicles, internal combustion engines, adaptive control, delay effects

I. INTRODUCTION

Triggered by the governmental regulations on emissions in 1960's and 1970's, the introduction of the microprocessor based control permitted the automotive manufacturers to design cleaner,

Y. Yildiz and A. M. Annaswamy are with the Department of Mechanical Engineering, Massachusetts Institute of Technology, Cambridge, MA, 02139 USA (e-mail: yildiray@mit.edu, aanna@mit.edu).

Diana Yanakiev and Ilya Kolmanovsky are with the Research and Innovation Center, Ford Motor Company, Dearborn, MI, 48121 USA (email: dyanakie@ford.com, ikolmano@ford.com).

Manuscript received November ??, 2008; revised January ??, 2009.

more fuel efficient, better performing and more reliable powertrain systems. The associated control problems provide continuing challenges to control engineers as the requirements progressively become more stringent. Higher levels of performance and robustness are expected, while the calibration time and effort need to be reduced. Advances in control theory can be exploited to address these challenges. See [1] for an introduction to modeling and control of internal combustion engines.

The Fuel-to-Air Ratio (FAR) control is one of the most important control problems for conventional gasoline engines. The FAR control performance can strongly impact key vehicle attributes such as emissions, fuel economy and drivability. For instance, the FAR in engine cylinders must be controlled in such a way that the resulting exhaust gases can be efficiently converted by the Three-Way Catalyst (TWC). The TWC efficiency is about 98 percent when the fuel is matched to air charge in stoichiometric proportion and drops abruptly outside a narrow region as seen in Fig. 1 [2]. The TWC can also compensate for the temporary FAR deviation from stoichiometry, by either storing excess oxygen or releasing oxygen to convert excess hydrocarbons (HC) and carbon monoxide (CO). Thus, for the TWC to operate efficiently, the stored oxygen level must be regulated so that a range to accommodate further release or storage during transient conditions is available [1]. The oxygen storage level in the TWC may be inferred on the basis of the TWC model and a signal from a switching Heated Exhaust Gas Oxygen (HEGO) sensor located downstream of the TWC. In addition, the oxygen storage capacity of the TWC depends on the size and precious metal loading of the TWC. Therefore, if the FAR excursions and their durations are reduced with a well-performing controller, the storage capacity of TWC and its cost may be reduced as well.

A conventional FAR control system includes two nested controllers. The outer-loop controller generates a reference FAR (set-point) for the inner-loop controller based, for instance, on the deviation of the estimated TWC stored oxygen state. The inner-loop controller maintains the FAR upstream of the TWC at this set-point by using the measurements of the feedgas FAR with a linear Universal Exhaust Gas Oxygen (UEGO) sensor to appropriately correct engine fueling rate. Small amplitude low frequency periodic modulation may be superimposed over the set-point to further improve catalyst efficiency. The HEGO sensor downstream of the TWC is also used to improve robustness to UEGO sensor drifts, changes to fuel type, and for diagnostics.

The inner loop controller consists of a feedforward component which is fast but may not

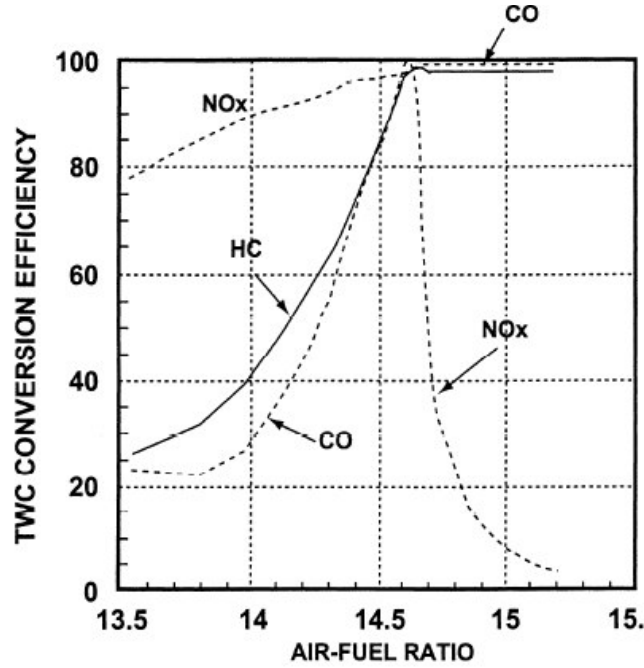


Fig. 1. TWC efficiency vs. air-to-fuel ratio.

be always accurate, and a feedback component which is slower but eliminates the steady-state error [1]. The feedforward component consists of estimation of the air and fuel path dynamics combined with appropriate compensations. These air and fuel dynamics correspond, mainly, to the intake manifold lag that affects the air charge, and the wall-wetting (WW) that determines the amount of fuel inducted into the cylinder for each fuel injection event during transient operation.

The FAR control problem has been extensively investigated over many years. In terms of advanced approaches, here we mention the use of nonlinear feedforward controllers [3], adaptive controllers [4], [5], [6], [7], feedback linearization [8], observer based controllers [9], [10], [11], sliding mode controllers [12], [13], [14], linear quadratic regulators [15], [16], H_∞ controllers [17], [18], Smith Predictors [19], neural network controllers [20] and model predictive controllers [21]. The use of an electronic throttle as an additional control actuator [22] or secondary/port throttles [23] has been also explored. Apart from stoichiometric FAR controllers, reference [24] considers control of FAR in a lean burn engine using linear parameter-varying controllers. In addition to these control research, [25] presents an interesting example of estimating the FAR in the cylinders without using the oxygen sensor and thus reducing the time delay in the system,

and [26] presents a research result on estimating the fuel-film dynamics. The motivation for these and related studies has been to achieve improved performance and robustness of the FAR control thereby enabling emission, fuel economy and drivability improvements.

Main challenges in the design of the FAR controller include variable time delay, uncertain plant behavior and disturbances. The time delay in the system comprises two basic components [24]: the time it takes from the fuel injection calculation to exhaust gas exiting the cylinders and the time it takes for the exhaust gases to reach the UEGO sensor location. The time delay in the system is a key factor limiting the bandwidth of the FAR feedback loop. The plant uncertainties are the result of inaccuracies in the air charge estimation and in the WW compensation, as well as changes in the UEGO sensor due to aging. When the carbon canister, which stores the fuel vapor generated in the fuel tank, is purged, the fuel content in the purge flow into the intake manifold is also uncertain and creates disturbance to the FAR control loop.

We, therefore, are interested in a control approach which can handle both uncertainties and large time-delays, and that can achieve a high performance. Literature, given above, about classical and advanced control applications to the FAR control problem proves the success of an automatic, model based control approach, and our work built upon these results by eliminating the need of a precise engine model for classical or optimization based algorithms and by eliminating the conservatism introduced by the robust control approaches. This is achieved by using the Adaptive Posicast Controller (APC) [27], [28], which is an adaptive controller for time delay systems. Successful adaptive control approaches are presented also in references [4], [5], [6] and [7], but our approach is different from them: In [4] and [6], a nonlinear least squares parameter identification method is used to identify the plant parameter values online and then use these values in the controller. For the convergence of these parameters, the condition of persistent excitation is needed. In addition, this online parameter identification may require extra computational power. In both of the references, the controllers are applied to a single cylinder laboratory engine. In [5], again a similar approach is taken where an extended Kalman Filter is used to identify the plant parameter values online. Similarly, in [7], the authors use a step by step experimental procedure to identify the sensor time constant, during the time of operation, where a rich input excitation is needed for parameter convergence. Our approach is based on direct adaptation where an online parameter identification scheme is not used. In addition, we apply the APC to a Lincoln Navigator test vehicle with 8 cylinders, which makes the control

task much harder due to cylinder to cylinder variations. Finally, in our work, we do not only present our results but also give a comparison with the existing control design in the test vehicle and with a gain scheduled Smith Predictor.

The Adaptive Posicast Control (APC) is a recently developed control design approach that is especially suited for plants with large time-delays [27], [28] and parametric uncertainties. The APC can be described as an adaptive controller that combines explicit delay compensation, using the classical Smith Predictor [29] and finite spectrum assignment [30], and adaptation [31], [32]. Due to such a unique combination, the APC effectively deals with both uncertainties and large time-delays both of which are dominant features of the FAR control problem. Previously, the authors explained preliminary implementation results of this controller to idle speed control and FAR control problems in conference papers [33], [34] and [35]. This paper expands on those results with further theoretical improvements, new experimental results and more detailed explanations of the experimental issues.

To fit the specific needs of the FAR application, our design has been extended with additional features: First, an adaptive feedforward term is added which is crucial for disturbance rejection. Second, procedures are developed for the controller parameter initialization and the adaptation rate selection to reduce the calibration time and effort. Third, an algorithm to take care of the variable delay is introduced. Fourth, an anti-windup logic is used to prevent the winding up the integrators used for parameter adaptation. Finally, a robustifying scheme is used to prevent the drift of the adaptive parameters. Our main contribution is the demonstration of the potential of this adaptive controller to improve the performance and to reduce the time and effort required for the controller calibration. This is achieved by the help of modifications and improvements that are listed above.

The experimental results obtained using a Lincoln Navigator test vehicle provided by Ford Motor Company, Dearborn, USA, demonstrate the capability of the controller to improve performance and decrease the calibration time and effort.

Adaptive Posicast FAR control approach represents a step towards a fully self-calibrating FAR controller because it reduces reliance on feedforward characterization and because the controller gains are automatically tuned online.

For comparison with the APC, we also develop in this paper a feedforward adaptive controller that attempts to minimize the impact of the purge fuel disturbance. We also compare this

controller with the baseline controller using simulations and in-vehicle experiments.

While our control approach is adaptive, its development both benefits from and depends on the structural properties of the underlying plant model. This plant model for FAR ratio control is briefly discussed next, while the reader is referred to [1] for a more extended treatment of the underlying modeling techniques.

II. PLANT MODEL

A block diagram representation of the plant, from fuel injection to the universal exhaust gas oxygen (UEGO) sensor measurement, together with the TWC is shown in Fig. 2, where “ A ” stands for the air charge that is calculated based on the driver torque command. The fuel inducted into the engine cylinders is viewed as the sum of the output the WW dynamics block and the canister purge, while the fuel injected by the injectors is an input to the WW block. The multiplication by the gain in the “ $1/A$ ” block gives the FAR of the mixture in the engine cylinders (we will consider the control of FAR as opposed to air-to-fuel ratio (AFR) since it scales linearly with fuel) and the delay block represents the combined effect of time delays in the system. The largest contributors to that delay are the time from the fuel injection to exhaust gas formation and the time needed for the exhaust gases to reach the UEGO sensor location. Finally, the exhaust gases undergo mixing, FAR is measured by the UEGO sensor and then the mixture passes through the TWC to get stripped from its pollutants.

In the model we use, the input is the mass flow rate of fuel injected by the injectors and the output is the equivalence ratio, which is the fuel to air ratio normalized by its stoichiometric value, measured by the UEGO sensor in the exhaust. As explained above, there are mainly four components of the FAR dynamics which are wall-wetting dynamics, fuel-air mixture formation, mixture propagation to the UEGO sensor location and finally UEGO sensor dynamics. Below, the modeling aspects for each component together with their transfer functions are explained.

A. Wall-Wetting (WW) Dynamics

After the fuel is injected by the injectors, some of the fuel immediately evaporates and is inducted into the engine cylinders, while the rest replenishes a liquid fuel puddle, which forms on the walls of the intake ports and on the intake valves. A fraction of the fuel evaporates

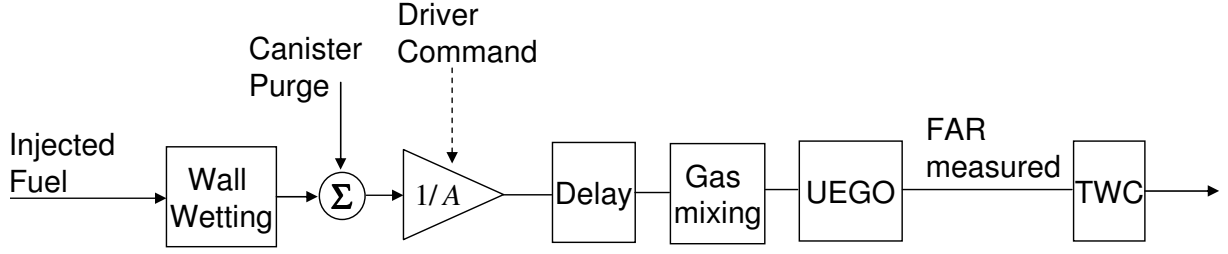


Fig. 2. Plant block diagram representation.

from the liquid puddle and is also inducted into the engine cylinders. A WW dynamics model represents this phenomenon with the following transfer function.

$$\frac{F_c(s)}{F_i(s)} = \frac{1 + (1 - X)\tau_{vs}}{\tau_v(s) + 1} \quad (1)$$

where F_c , F_i , X and τ_v represent the fuel entering the cylinders, injected fuel, the fraction of the fuel contributing to the fuel puddle and the puddle evaporation time constant, respectively.

B. FAR Formation and Propagation to the UEGO Sensor

The vaporized fuel mixes with the air and forms the fuel-air mixture. This process may be modeled as a division of the fuel mass by the air mass, $A(t)$, entering the cylinder. Starting from the opening of the intake valve, it takes approximately one engine cycle, i.e., 2 crankshaft revolutions, until the exhaust gases fully exit the cylinder. This delay is called the cycle delay, τ_c , and can be approximated as $\tau_c = 120/N$, where N is the engine speed in revolutions-per-minute.

After the exhaust gases exit the cylinder, they mix with the previously existing exhaust gases and travel through the exhaust manifold until they reach the UEGO sensor location. Also, in a multi-cylinder engine, the exhaust gases coming from the individual cylinders enter the exhaust manifold at different times. All these effects can be modeled by a pure delay element in series with a first order lag as

$$\frac{\Phi_{bm}(s)}{\Phi_{eng}(s)} = \frac{1}{\tau_{gm}(s) + 1} e^{-\tau_{tr}} \quad (2)$$

where, Φ_{bm} , Φ_{eng} , τ_{gm} and τ_{tr} represent the equivalence ratio, which is fuel-to-air ratio divided by stoichiometric (desired) fuel-to-air ratio, just before the measurement, equivalence ratio right after the engine exit, gas mixing time constant and transport delay, respectively.

C. Sensor Dynamics

Sensor dynamics can be modeled by a first order lag as

$$\frac{\Phi_m(s)}{\Phi_{bm}(s)} = \frac{1}{\tau_s(s) + 1} \quad (3)$$

where $\Phi_m(s)$ and τ_s represent the measured equivalence ratio and sensor time constant, respectively.

D. Reduced Order Model

When all the individual elements of FAR dynamics described in eqns. (1)-(3) are combined, a third order transfer function in series with a pure delay is obtained. To simplify the controller design, a first order lag in series with a pure time delay is used as a reduced order plant model, where the input and the output are the deviations in the commanded in-cylinder equivalence ratio and the measured equivalence ratio.

$$G(s) = \frac{1}{\tau_m s + 1} e^{-\tau s} \quad (4)$$

Accurate WW compensation (effectively, the feedforward inversion of (1)) helps to render this approximation more valid. Using relay feedback identification method for time delay systems [36] the coefficients of this model at around the speed of 700 rpm and in warm conditions are found to be 0.4 and 0.45 for τ_m and τ , respectively. Note that τ consists of the cycle delay τ_c and the transport delay τ_{tr} and it also accounts for the UEGO sensor time delay and the computational delay in the engine control unit.

III. CONTROLLER DESIGN

The structure of the closed loop system used in the test vehicle is presented in Fig. 3. The figure shows the inner and the outer control loops. The outer loop determines the desired FAR, $(F/A)_d$, depending on the state of the TWC, measured by the HEGO sensor. $(F/A)_d$ becomes the reference for the inner loop controller or the feedback controller, which is referred to as “Controller”. The air estimate, referred to as \hat{A} , depends on the driver torque request. The multiplication of $(F/A)_d$ with \hat{A} is referred to as the “base fuel”, F_b , which is an estimate of the desired fuel. The feedback controller corrects this estimate using the UEGO sensor measurement of the FAR upstream of the TWC. Note that the feedback controller applies a

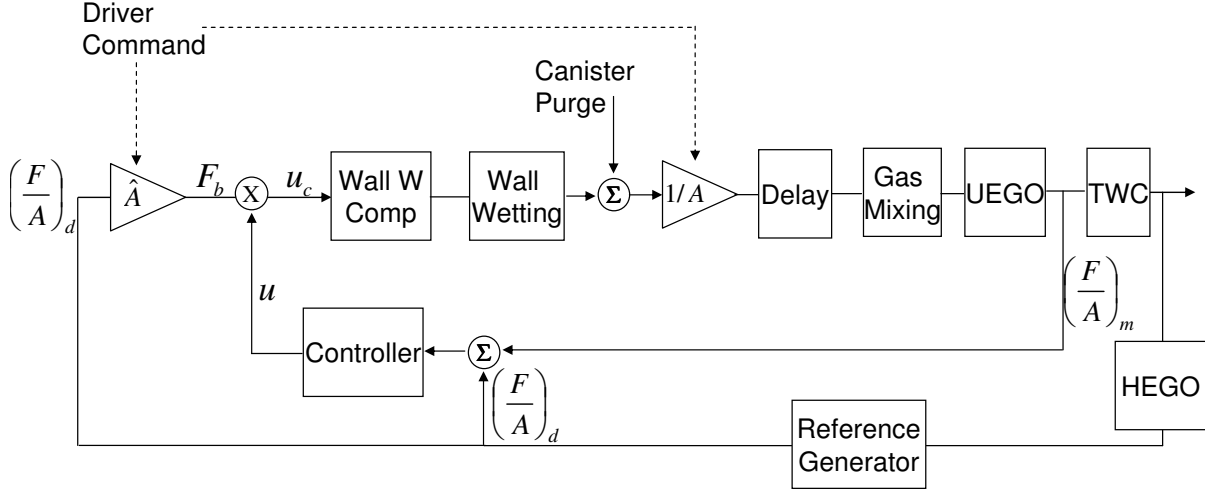


Fig. 3. Overall closed loop controller structure.

multiplicative correction as opposed to additive correction, although the latter is more typical in controls literature. The advantage of the multiplicative feedback over additive feedback is that the feedback fuel quantity scales proportionally to the value of the base fuel thereby providing better ability to compensate in transients when changes in vehicle operating point occur as this multiplicative transformation maintains the dc gain of the Plant assumed for fuel-to-air ratio feedback design constant across the vehicle operating range. In addition to the feedback controller there is a WW compensation algorithm in the system which estimates the WW dynamics and use the inverse dynamics to cancel it.

What we are interested in is the feedback controller, for which we design two different adaptive controllers with different complexity. Before explaining these designs, we explain the baseline controller first, which is the existing feedback controller in the vehicle.

A. Baseline Controller

The baseline controller in the vehicle is essentially a gain-scheduled Proportional-plus-Integral (PI) controller. In the actual vehicle implementation, a first-order filter in series with PI controller and relay logic are used. Note that before the feedback control input is multiplied by the base fuel F_b , it is shifted by 1. So the resulting control input for the baseline controller can be given

as

$$u_c = (1 + u)F_b, \quad (5)$$

where u_c is the total control signal without the WW compensation and u is the output of the feedback controller. This structure has the advantage of a feedback control input u that has relatively small values, since its bias, 1, is already causing the control signal u_c to be equal to the required base fuel F_b .

Note that, to maintain stability in the presence of delay, the gains of the PI controller cannot be made very aggressive. Moreover, due to the delay in the system, the overshoot in the response is difficult to avoid using this feedforward-feedback combination.

B. Adaptive Feedforward Controller (AFFC)

The system diagram with the Adaptive Feedforward Controller (AFFC) is shown in Fig. 4. This is a simple model reference adaptive controller, where it is assumed that the only uncertainty occurs in the control input gain. Instead of the feedback path in Fig. 3, a gain multiplier on the $(F/A)_d$ is adapted. Note that the outer loop is not shown in the figure. The motivation for AFFC is to compensate for errors in the base fuel calculation due to, for example, injector uncertainties or “lost-fuel” effects present at cold engine conditions. Assuming that the desired FAR is in general constant and equal to stoichiometric FAR, it can be shown that this controller can also reject constant disturbances.

To derive the adaptation law, consider the following reduced order plant model represented in state space form with a constant disturbance

$$\dot{x}_p = ax_p + b(u(t - \tau) + d) \quad (6)$$

where, x_p represents the measured FAR, a and b are known and unknown constants respectively and d is a constant, unknown disturbance. Since the plant is stable, a is negative and since b represents the gain of the injectors, it is positive. Note that since reduced order dynamics is first order, (6) is a scalar differential equation.

Consider a reference model

$$\dot{x}_m = ax_m + b_m r(t - \tau) \quad (7)$$

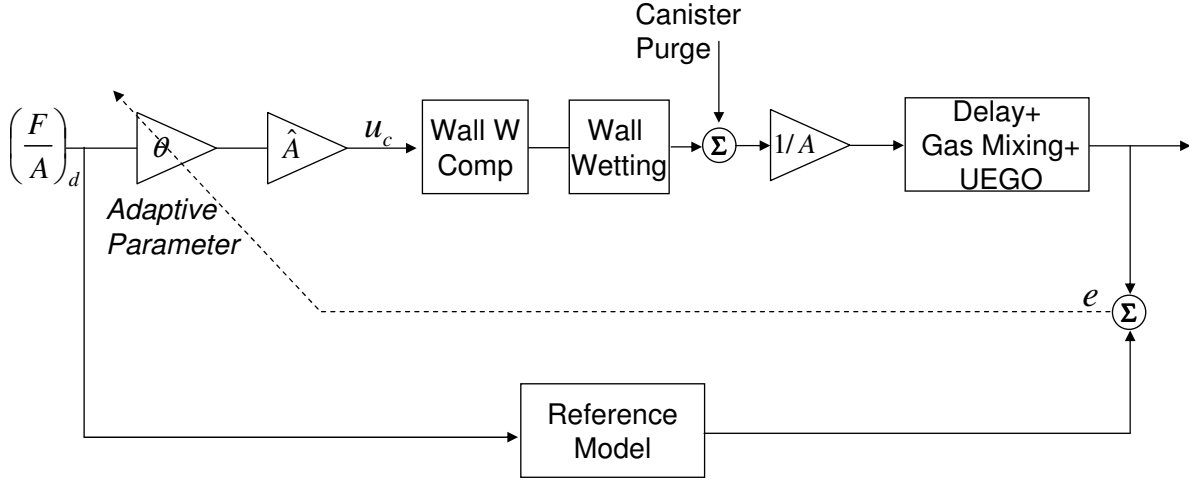


Fig. 4. Inner-loop structure with AFFC.

where r is the desired FAR or $(F/A)_d$. Assuming that the reference FAR is constant so that $r = r_0$, we choose the control input as

$$u = \theta r_0 = (\theta^* + \tilde{\theta}(t))r_0 \quad (8)$$

where $\theta^* = b_m/b - d/r$ is the ideal controller parameter and $\tilde{\theta}$ is the deviation of θ from θ^* . By using a Lyapunov function candidate $V = (e^2 + b\tilde{\theta}^2)/2$, it can be shown that $\tilde{\theta}(t)$ is bounded and $\lim_{t \rightarrow \infty} e(t) = 0$, if the following update law is used

$$\dot{\tilde{\theta}} = \dot{\theta} = -\gamma e r \quad (9)$$

where γ is the adaptation rate and $e = (F/A)_m - (F/A)_{rm}$. Here $(F/A)_m$ and $(F/A)_{rm}$ represents the measured FAR and the output of the reference model.

One of the advantages of AFFC is providing a more damped response compared to the baseline controller when the goal is reference tracking. In addition AFFC is easier to tune since it has only one parameter. Note that an adaptation law (9) can be enhanced with a dead-band or a sigma-modification and with a projection algorithm.

C. Adaptive Posicast Controller (APC)

As discussed above, AFFC can handle the uncertainties in the controller gain. However, in reality there are more uncertainties in the system resulting from, for example, the actuator aging or simply from the operating point changes such as varying temperatures, speeds and loads. All these effects can change the system dominant pole. Therefore, we need a controller that can also adapt to these uncertainties, and that makes the APC a good candidate.

APC is a model reference adaptive controller for systems with known input delay. Below, we summarize the main idea behind the APC. The reader is referred to [28] for additional details. Consider a linearized plant with input-output description given as

$$y(t) = W_p(s)u(t - \tau), \quad W_p(s) = \frac{k_p Z_p(s)}{R_p(s)} \quad (10)$$

where y is the measured plant output, u is the control input, and $W_p(s)$ is the delay-free part of the plant transfer function. $R_p(s)$ is the n^{th} order denominator polynomial, not necessarily stable and the numerator polynomial, $Z_p(s)$ has only minimum phase zeros. The relative degree, n^* , which is equal to the order of the denominator minus the order of the numerator, is assumed to be smaller or equal to two. It is also assumed that the delay and the sign of the high frequency gain k_p are known, but otherwise $W_p(s)$ may be unknown. Suppose that the reference model, reflecting desired response characteristics, is given as

$$y_m(t) = W_m(s)r(t - \tau), \quad W_m(s) = \frac{k_m}{R_m(s)} \quad (11)$$

where $R_m(s)$ is a stable polynomial with degree n^* , k_m is the high frequency gain and r is the desired reference input.

Consider the following state space representation of the plant dynamics (10), together with two “signal generators” formed by a controllable pair Λ, l

$$\dot{x}_p(t) = A_p x_p(t) + b_p u(t - \tau), \quad y(t) = h_p^T x_p(t) \quad (12)$$

$$\dot{\omega}_1(t) = \Lambda \omega_1(t) + l u(t - \tau) \quad (13)$$

$$\dot{\omega}_2(t) = \Lambda \omega_2(t) + l y(t) \quad (14)$$

where, $\Lambda \in \mathbb{R}^{n \times n}$ and $l \in \mathbb{R}^n$. It follows [37] that there exist $k^* \in \mathbb{R}$, $\alpha_1^{*T}, \alpha_2^{*T} \in \mathbb{R}^n$, $\lambda^*(\sigma) :$

$[-\tau, 0] \rightarrow \Re$ such that the control law

$$\begin{aligned} u(t) = & \alpha_1^{*T} \omega_1(t) + \alpha_2^{*T} \omega_2(t) + \int_{-\tau}^0 \lambda^*(\sigma) u(t + \sigma) d\sigma \\ & + k^* r(t). \end{aligned} \quad (15)$$

satisfies the exact model matching condition.

$$\frac{y(t)}{r(t)} = \frac{k_m}{R_m(s)} e^{-\tau s}. \quad (16)$$

We now consider the control of the plant (10) when the transfer function $W_p(s)$ has unknown coefficients and the time delay τ is known. Consider the following adaptive controller [28]:

$$\begin{aligned} u(t) = & \alpha_1(t)^T \omega_1(t) + \alpha_2(t)^T \omega_2(t) + \int_{-\tau}^0 \lambda(t, \sigma) u(t + \sigma) d\sigma \\ & + k(t) r(t), \\ \dot{\theta}(t) = & -\Gamma e_1(t) \Omega(t - \tau), \\ \frac{\partial \lambda(t, \sigma)}{\partial t} = & -\gamma_\lambda(\sigma) e_1(t) u(t + \sigma - \tau) \end{aligned} \quad (17)$$

where,

$$\theta = \begin{bmatrix} \alpha_1 \\ \alpha_2 \\ k \end{bmatrix}, \quad \Omega = \begin{bmatrix} \omega_1 \\ \omega_2 \\ r \end{bmatrix}, \quad e_1 = y - y_m, \quad (18)$$

Γ is a diagonal matrix, the entries of which represent the adaptation rate of the corresponding controller parameter and $\gamma_\lambda(\sigma)$ is the adaptation rate for the controller parameter $\lambda(t, \sigma)$. Defining the parameter errors as $\tilde{\theta}(t) = \theta(t) - \theta^*$, $\tilde{\lambda}(t, \sigma) = \lambda(t, \sigma) - \lambda^*(\sigma)$, the control signal u in (17) can be rewritten as

$$\begin{aligned} u(t) = & \alpha^{*T} \omega(t) + \int_{-\tau}^0 \lambda^*(\sigma) u(t + \sigma) d\sigma \\ & + k^* r(t) \\ & + \tilde{\alpha}(t)^T \omega(t) + \int_{-\tau}^0 \tilde{\lambda}(t, \sigma) u(t + \sigma) d\sigma \\ & + \tilde{k}(t) r(t) \end{aligned} \quad (19)$$

where $\alpha \triangleq [\alpha_1 \ \alpha_2]$. It is shown in [28] that the differential equations, (12), (13), (14) together with the control signal (19) describe the closed loop dynamics as

$$\begin{aligned}\dot{X}_p(t) &= A_m X_p(t) + b_m [\tilde{\alpha}^T(t - \tau) \omega(t - \tau) \\ &+ \int_{-\tau}^0 \tilde{\lambda}(t - \tau, \sigma) u(t - \tau + \sigma) d\sigma + \tilde{k}(t - \tau) r(t - \tau) + k^* r(t - \tau)], \\ y_p(t) &= h_m^T X_p(t)\end{aligned}\tag{20}$$

where, $X_p \triangleq [x_p^T \ \omega_1^T \ \omega_2^T]^T$, $h_m^T \triangleq [h_p^T \ 0 \ 0]$, $y_p = y$ and A_m is a constant Hurwitz matrix. From the model matching condition, we know that when the parameter errors are equal to zero, the closed loop transfer function is identical to that of the reference model. Therefore, the reference model can be described by the $(3n)^{\text{th}}$ order differential equation

$$\dot{X}_m(t) = A_m X_m(t) + b_m k^* r(t - \tau), \quad y_m(t) = h_m^T X_m(t)\tag{21}$$

where,

$$\begin{aligned}X_m(t) &\triangleq [x_p^{*T} \ \omega_1^{*T} \ \omega_2^{*T}]^T, \\ h_m^T (sI - A_m)^{-1} b_m k^* &= \frac{k_m}{R_m(s)}.\end{aligned}\tag{22}$$

Note that $x_p^*(t)$, $\omega_1^*(t)$ and $\omega_2^*(t)$ can be considered as the signals in the reference model corresponding to $x_p(t)$, $\omega_1(t)$ and $\omega_2(t)$ in the closed loop system. Therefore, subtracting (21) from (20), we get an error equation for the overall system as

$$\begin{aligned}\dot{e}(t) &= A_m e(t) + b_m [\tilde{\alpha}^T(t - \tau) \omega(t - \tau) \\ &+ \int_{-\tau}^0 \tilde{\lambda}(t - \tau, \sigma) u(t - \tau + \sigma) d\sigma \\ &+ \tilde{k}(t - \tau) r(t - \tau)], \\ e_1(t) &= h_m^T e(t).\end{aligned}\tag{23}$$

where $e(t) = X_p - X_m$ and $e_1(t) = y_p(t) - y_m(t)$. Equation (23) can be written in a more compact form as

$$\begin{aligned}\dot{e}(t) &= A_m e(t) + b_m [\tilde{\theta}^T(t - \tau) \Omega(t - \tau) \\ &+ \int_{-\tau}^0 \tilde{\lambda}(t - \tau, \sigma) u(t - \tau + \sigma) d\sigma] \\ e_1(t) &= h_m^T e(t).\end{aligned}\tag{24}$$

Using the error model (24) and defining an appropriate Lyapunov Krasovskii functional, it can be shown [28] that the plant (10), adaptive controller and the adaptive laws given in (17) have bounded solutions for all $t \geq t_0$ and $\lim_{t \rightarrow \infty} e_1(t) \rightarrow 0$.

D. Implementation Enhancements

In order to implement the Adaptive Posicast Controller specified by (13), (14) and (17), one has to address several issues which were not taken into account during the initial design but arise in the implementation. Below, we explain these issues and how we address them.

1) *Disturbance rejection:* Controller (17) is a model reference adaptive controller where the goal is to force the plant output follow the reference model output. In the design stage, the input disturbances are not explicitly taken into account. However, in the FAR control application, it can be shown that the controller is rejecting constant input disturbances. Indeed, the reference, FAR set-point, is constant for this application, which turns the feedforward term $k(t)r(t)$ into a pure integrator. Please see Appendix A for the proof of the disturbance rejection.

2) *Initialization and Adaptation Rate Selection:* We initialize our controller parameters by satisfying the model matching using a nominal plant model. For the nominal plant we choose 700 rpm as the engine speed at warm idling conditions. Idling can be considered as the worst case since the delay value achieves its maximum value. In this operating condition τ and τ_m is found to be 0.4 and 0.45 respectively.

We choose the adaptation gain $\bar{\Gamma}_{ii}$ for a particular controller parameter $\bar{\theta}_i$ using the following empirical rule

$$\bar{\Gamma}_{ii} = c\bar{\theta}_{i0} \quad (25)$$

where c is an adjustable gain and $\bar{\theta}_{i0}$ is the initial value of the corresponding controller parameter. Note that we use the same c for all the parameters which makes the fine tuning procedure easy and fast. The rationale for this rule is to make all the controller parameters equally effective in the control law.

3) *Approximation of the finite integral term:* The finite integral term in the control signal u given in (17) is implemented by using a set of point-wise delays [30] as in the following:

$$\int_{-\tau}^0 \lambda(\sigma, t) u(t + \sigma) d\sigma = \lambda_1(t) u(t - dt) + \dots + \lambda_m(t) u(t - mdt) \quad (26)$$

where dt is the sampling interval and $mdt = \tau$. With this approximation, the adaptive laws given in (17) can be represented as

$$\dot{\bar{\theta}}(t) = -\bar{\Gamma}e_1(t)\bar{\Omega}(t - \tau) \quad (27)$$

where,

$$\bar{\theta} = \begin{bmatrix} \alpha_1 \\ \alpha_2 \\ \lambda_1 \\ \vdots \\ \lambda_m \\ k \end{bmatrix}, \quad \bar{\Omega} = \begin{bmatrix} \omega_1 \\ \omega_2 \\ u(t - dt) \\ \vdots \\ u(t - mdt) \\ r \end{bmatrix}, \quad (28)$$

and $\bar{\Gamma}$ is the diagonal adaptation rate matrix.

In [38] the limitations of this approximation have been pointed out together with an example of unstable behavior arising due to numerical integration. In the powertrain control problem considered here, both in the experiments and in the simulations, the values of coefficients λ_i are in the order of 10^{-3} to 10^{-4} , and for these values the danger of the instabilities due to numerical approximation does not arise.

4) *Handling Time-Varying Delay:* In the design of the APC, it assumed that the time delay in the system is known and constant. However, the time delay in the FAR control problem varies with the load and the speed of the engine. A logical way of handling this issue is gain-scheduling the controller, time delay being the gain-scheduling variable. The delay value shows itself in the equation (13) and in the adaptation laws given in (17), which are straightforward to gain-schedule. Apart from these, the finite integral term in the control law given in (17) also needs the delay information to be computed. Note that we use an approximation for this term given in (26). We pursued two different strategies to gain-schedule this approximation, which are given below:

a) *Eliminating and Adding Terms:*

The integral in (26) is approximated using time steps that are equal to the sampling interval, T , of the controller implementation ($T = 30$ ms). Therefore, the number of the terms, m , in this approximation can be given as $m = \tau/T$. A simple way to gain-schedule this approximation is to eliminate or add terms, depending on the value of the delay at the time of approximation.

One can do this by storing the values of eliminated parameter λ_i 's when the delay decreases and then using these stored values when the number of the terms increases again, due to a delay increase.

Although this logic seems intuitive, it has a drawback of rapid control signal changes that can cause undesired excursions in the FAR trace.

b) Freezing and Adding Terms:

As we discussed above, when the delay value decreases, we need less parameters to approximate the finite integral in (26) and thus we eliminate the unnecessary terms. This causes a sudden, undesired jump in the control signal. To prevent this jump, instead of eliminating the unnecessary terms, $\lambda_i(t)u(t - idt)$'s, we simply freeze them and use them back when the delay value increases. This strategy achieves two things: First, it still makes sure that only the necessary terms are being used and thus only the necessary parameter λ_i 's are being updated, while the rest of them are frozen. Second, by still keeping the frozen terms in the control signal, it leads a smooth transition from one delay approximation to another.

Note that in the case of a delay decrease and thus freezing of the unnecessary terms, the control signal carries the frozen terms as a constant bias. Below, we show that this does not adversely effect the stability of the closed loop system.

Assume that the delay value τ decreased to τ' so that we need only need $p = \tau'/T$ terms instead of m terms to approximate the finite integral, where $p < m$. In this case, we freeze the $m - p$ unnecessary terms. Assume that the sum of these frozen terms are equal to D . The resulting approximation is the following:

$$\int_{-\tau'}^0 \lambda(\sigma, t)u(t + \sigma)d\sigma = \lambda_1(t)u(t - dt) + .. + \lambda_p(t)u(t - pdt) + D. \quad (29)$$

The state space description of the plant together with the controller given in (12) is now modified as

$$\dot{x}_p(t) = A_p x_p(t) + b_p(u(t - \tau) + D), \quad y(t) = h_p^T x_p(t). \quad (30)$$

We can, therefore, use the same procedure explained in Appendix A to show that the overall system stays stable and that the tracking error goes to zero.

5) *Anti-windup logic:* The fuel injector actuators, have their hard limits and the calculated control signal may sometimes exceed these limits, either from below or from above. Conse-

quently, an add-on algorithm needs to be integrated with the controller that prevents the winding up of the integrators resulting from the adaptation laws in (17).

We use anti-windup logic where the main goal is to stop the adaptation if the control signal saturates and if the tracking error, $e_1 = y_m - y_p$, is not favorable. Calling the control signal before the saturation block as u and after the saturation as u_{sat} , the anti-windup algorithm can be expressed as in the following.

$$\dot{\bar{\theta}}_i(t) = \begin{cases} 0 & \text{if } u > u_{\text{sat}} \text{ and } e_1 < 0 \\ \text{or} \\ u < u_{\text{sat}} \text{ and } e_1 > 0 \\ -\bar{\Gamma}_{ii}e_1(t)\bar{\Omega}_i(t - \tau) & \text{otherwise} \end{cases} \quad (31)$$

The additional tracking error based condition for not suspending the adaptation during saturation improved the speed of the transient response as has been demonstrated in our vehicle experiments.

There are more rigorous anti-windup methods that are specifically developed for adaptive controllers [39]. We plan to apply these methods in our future research.

6) *Robustness*: The adaptive controller design presented in Section III-C portrayed an idealized situation. The delay free part of the plant dynamics, $W_p(s)$, is assumed to be finite dimensional, linear and time invariant with unknown parameters. It is also assumed that the inputs and outputs to the plant can be measured exactly. However, in the real implementation, no plant is truly linear or finite dimensional. Plant parameters may vary with time and operating conditions, and measurements may be contaminated by noise. The plant model is almost always approximate. It is precisely in these cases that adaptive control is most needed [37].

Due to the above possible violations of the assumptions, the controller parameters may drift without converging to a bounded region. One of the remedies to this problem is using σ -modification robustness scheme [37], which mainly adds a damping term to adaptation laws. We previously used this robustness scheme in idle speed control application [40] which proved successful and therefore we used it again in FAR control application. Please see [40] for the details.

E. Final Design and Calibration

We believe that any controller design that is meant to be used in a mass-production application must be accessible and easy to use by the engineering staff who actually implements and supports the control strategy in production. This is particularly important given that the engineering staff are not expected to be highly skilled in advanced control methods. Motivated by these facts, below we give a step by step design procedure to obtain a transparent and streamlined design. We assume that a linear plant model with uncertain parameters and a known time delay is available.

- Step 1.* Select Λ and l of the signal generators defined in (13) and (14). These signal generators act like state observers and it is suggested that the eigenvalues are selected much faster than the reference model pole. Note that the Λ - l pair must be controllable.
- Step 2.* Set the initial value of the controller parameters by satisfying the model matching using a nominal plant model.
- Step 3.* Set the time constant of the reference model at least two times faster than that of the nominal plant time constant.
- Step 4.* Set the adaptation rate matrix Γ according to the algorithm given in (25).
- Step 5.* Tune the parameter c until the control requirements are satisfied. Note that increasing c gives a tighter FAR control performance, however higher gains might cause undesired oscillations.

Apart from these five easy steps, the design must be integrated with the robustness scheme as discussed in Section III-D-6.

Note that the controller needs only about 0.4KB of memory for the data storage and requires 118 number of operations per computation cycle. This corresponds to less than $4 \cdot 10^3$ operations per second. For conventional ECU's the APC controller use around 0.04 percent of the total computational power and that is negligible. Please see the appendix in [40] for the calculation of the memory requirements and computational complexity.

IV. SIMULATION AND EXPERIMENTAL RESULTS

The simulation results in this section are obtained using ®Matlab and ®Simulink, and the experimental results are obtained using a Lincoln Navigator test vehicle provided by Ford Motor Company. The vehicle has a 5.4 liter V-8 front engine with a multi-port fuel injection system.

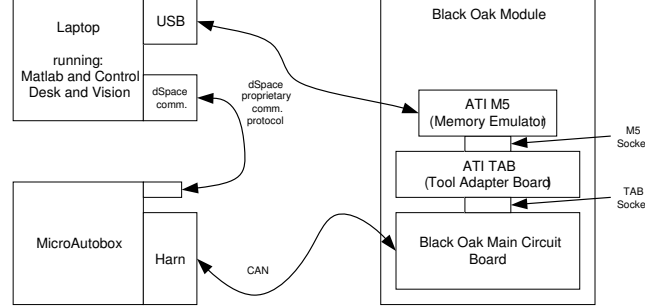


Fig. 5. Rapid prototyping with MicroAutobox using CAN.

The engine has three valves per cylinder and can achieve 300 Hp at 5000 rpm and 495 Nm at 3750 rpm. The air intake is controlled with an electronic throttle.

A dSPACE MicroAutoBox, communicating with the engine control unit (ECU) via CAN bus was used for real-time controller rapid prototyping. This system is used to implement the controller and monitor the performance. Figure 5 shows the hardware wiring. In the production environment, the engine is controlled by the ECU. The ECU normally also controls the other actuators of the engine, monitors the health of the engine and processes sensor inputs [41].

In our setup, we override the FAR control commands coming from the ECU with our adaptive control signal using the rapid prototyping system (see Figure 5). This system has the FAR as the measured input and calculates the fuel mass flow rate as the control input.

The existing closed loop control structure in the vehicle is presented in Fig. 3. The adaptive controller overwrites the “Controller” block, while the rest of the structure is retained as is. Thus, our results compare the performance of the existing feedback controller in the test vehicle with the adaptive controller. It was observed that the Adaptive Posicast Controller performed better when compared to the existing baseline controller, in all experiments.

A. AFFC vs. Baseline Controller

Figure 6 compares the tracking and purge disturbance rejection performance of the baseline controller and of the AFFC when WW dynamics are assumed to be perfectly compensated. Φ denotes the normalized FAR or the equivalence ratio (so that stoichiometric FAR of 0.0685 corresponds to $\Phi = 1$). The upper plot shows the simulated response to a pulse train reference

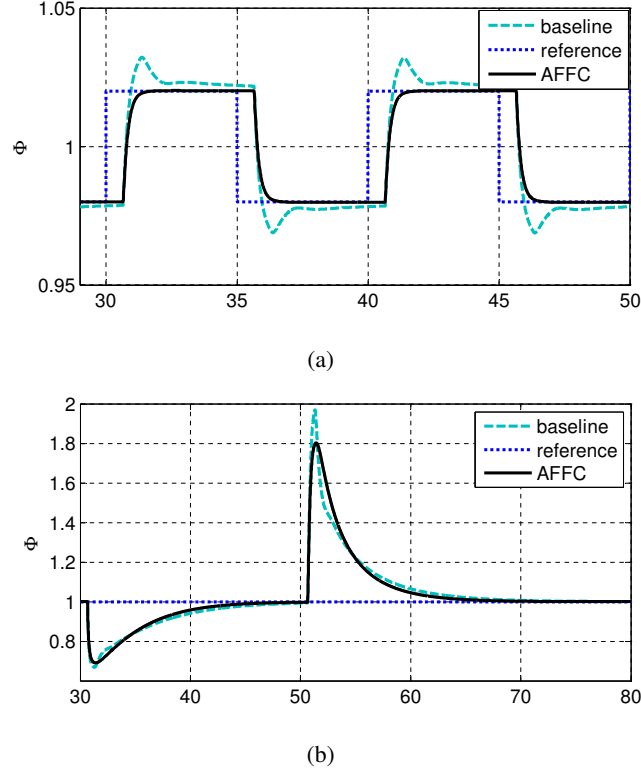


Fig. 6. Comparison of baseline controller and AFFC. a) Response to a set-point change b) Response to purge disturbance.

and the lower plot shows the response to a step purge disturbance introduced at time $t = 30$ sec and removed at time $t = 50$ sec. It is assumed that the time delay is known to be 0.4 sec. While designing the AFFC, the UEGO dynamics are assumed to have nominal values but then the plant dynamics were chosen to have 20 percent deviations in high frequency gain and τ_m . The baseline controller is tuned to perform well for both tracking and disturbance rejection. As discussed before, the baseline controller cannot avoid overshoots due to the delay in the system, while the AFFC can track the reference comparatively better. On the other hand, the disturbance rejection capabilities are similar, since when the reference is constant, the AFFC is essentially an integral controller.

We have also tested AFFC experimentally and compared it with the existing baseline controller. At the test time, the calibration of WW compensation was not fully completed, which allowed to subject both controllers to challenging scenarios. Also, the time delay varied in the experiments as opposed to the cases simulated in Fig. 6. Figure 7 shows the results from a 4-minute drive

test. Note that the air charge values have been scaled to show them in the same plot with Φ . The test was conducted in a relatively uncontrolled environment, e.g., without controlling the speed or load, as can be observed in Figs. 7a-c. The vehicle was accelerated and decelerated rather sharply and the purge flow was also not controlled, as shown in Fig. 7-d. The RMS error value of the deviations from the reference is calculated as 0.0052 and 0.0051 for the baseline controller and for the AFFC, respectively. Their performances are similar, consistently with our simulation results, as the dominant factors affecting the response are the purge and air disturbances, and not the reference tracking.

Note that another important success measure (SM) for the FAR control loop is the error integral. Compared to RMS error, this metric better reflects how much of the TWC oxygen storage capacity is used to compensate for the deviations in the fuel-to-air ratio.

The integral error SM can be formulated as

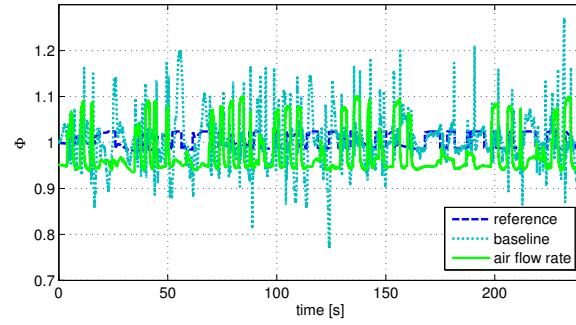
$$SM = \frac{1}{k} \sum_{i=1}^k \left| \int_{t_i}^{t_i + \Delta_i} e_1(\eta) d\eta \right| \quad (32)$$

where t_i is the time instant of the i -th disturbance hit and Δ_i is the duration/settling time of the transient caused by the disturbance hit. We use this SM for the APC results in the following sections.

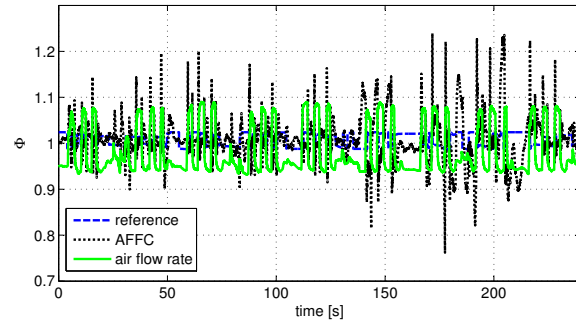
B. APC vs. Baseline Controller

1) Purge Disturbance Rejection Tests: The purpose of our initial FAR control experiments was to compare the performances of the APC and the baseline controller, while emulating canister vapor purge disturbance rejection tests. These experiments were conducted with the test vehicle idling at different speeds. Since during idling the air flow rate does not change much, the WW dynamics did not play a major role in these experiments as much as it did for acceleration and deceleration experiments. The SM used is given in (32).

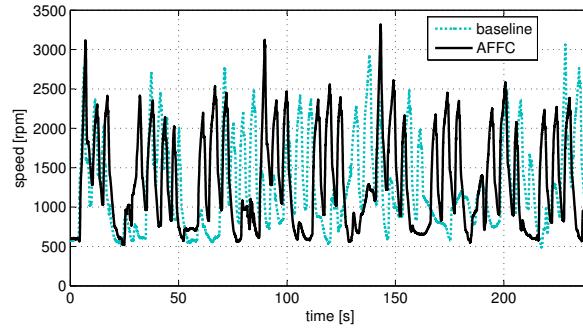
The test started with the engine speed at 700 rpm. At 300 sec, the engine speed increased to 1000 rpm and at 600 sec it decreased back to 700 rpm. Every 20 sec the fuel injector gains were changed to emulate the purge disturbance. Overall, the performance of the APC, calculated using (32), was 70 percent better than the baseline controller during the test which lasted 15 minutes. Figure 8 shows a time window from the test where the engine speed was 700 rpm.



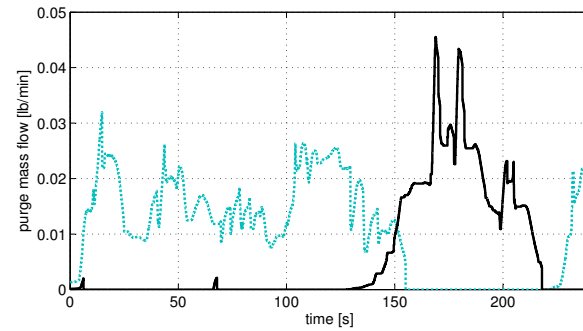
(a)



(b)



(c)



(d)

Fig. 7. Baseline controller vs. AFCC a) Φ and air flow rate when baseline controller is active b) Φ and air flow rate when AFCC is active c) Engine speeds d) Purge fuel flow rates.

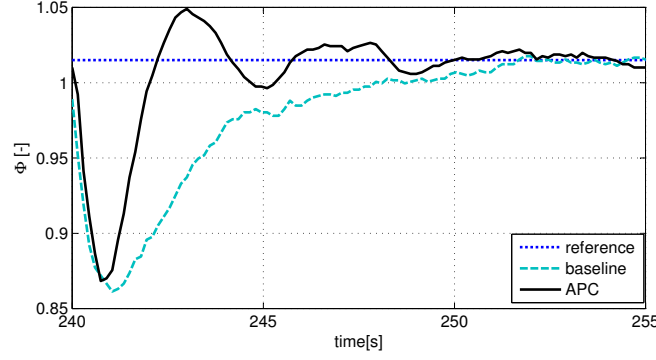


Fig. 8. Comparison of baseline controller with APC for purge disturbance rejection at 700 rpm.

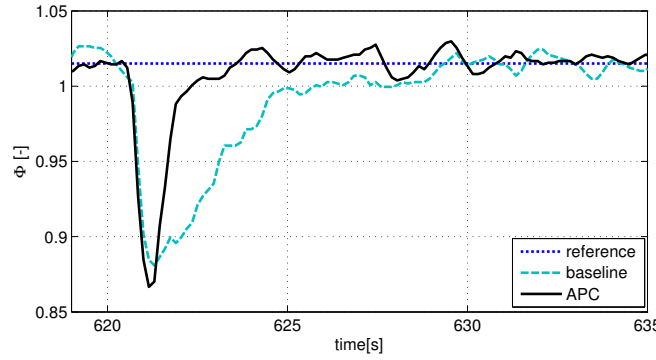


Fig. 9. Comparison of baseline controller with APC for purge disturbance rejection at 1000 rpm, with $c = 1$.

The APC performs considerably better, in terms of integral SM, than the baseline controller as its features enable it to better account for the delay and achieve faster response.

Figure 9 shows how the equivalence ratio changes during the same test but now the engine speed is 1000 rpm. Again, the performance of the APC is better than that of the baseline controller.

2) *Acceleration and Deceleration Tests:* Figure 10 shows the equivalence ratio excursions during a test in which the vehicle accelerates and then decelerates. In this case, the delay varies with time during the test. The APC performs better overall than the baseline controller. During the lean excursion (equivalence ratio less than 1 during acceleration), the baseline controller appears to start the recovery from the undershoot slightly earlier than the APC. There are, however, differences in the air flow and the equivalence ratio set-point time of increase between

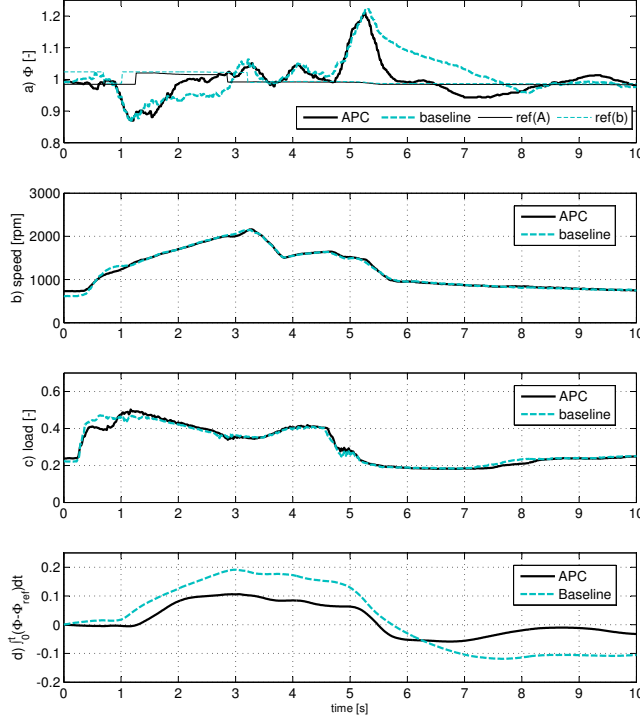


Fig. 10. Time histories of a) Φ , b) Engine speed c) Engine relative air flow, d) Tracking error integral, during vehicle acceleration and deceleration for APC vs. baseline controller, with $c = 1$.

APC test and baseline controller test, further analysis of these suggests no real advantage for the baseline controller over APC in terms of start of recovery timing. Note that the equivalence ratio set-point is computed by a separate part of the engine control system in the vehicle.

For this experiment, we compared the maximum value of the integrated difference between fuel-air equivalence ratio and its set point during the full course of the experiment. This metric is better suited to assessing the difference between controllers for this experiment than (32) because if one acceleration-deceleration test is assumed to be a single event, the errors cancel each other if (32) is used, which can be observed in (10)-d. However, maximum value of the integral relates to how much of the oxygen storage capacity is used in the worst case during the course of the experiment. In terms of this metric, APC performs 43 percent better than the baseline controller.

All the above experiments were conducted with the fine tuning parameter c equal to 1, which implies that no fine-tuning was done. In Fig. 11, we present an experimental result, which shows

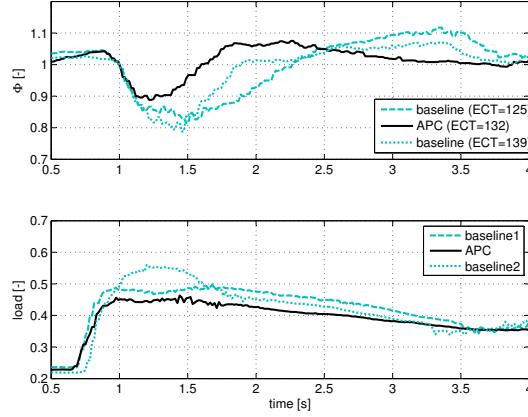


Fig. 11. Comparison of baseline controller with APC during vehicle acceleration, with $c = 1.5$.

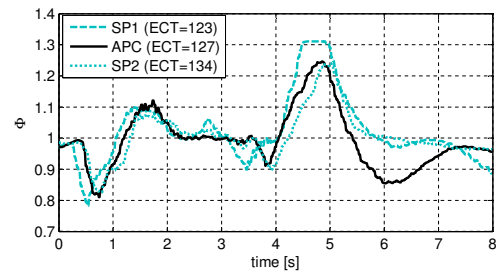
APC and the baseline controller performances during the vehicle acceleration, with $c = 1.5$. As expected, the APC outperforms the baseline controller to a greater extent compared to the previous cases, especially on lean excursions. Note however that the load (and hence the air charge) are less in the APC controller case in this experiment. Nevertheless, performance with the APC is considerably better than with the baseline controller, and cannot be attributed to the load difference between the controllers.

C. APC vs. Gain-Scheduled Smith Predictor

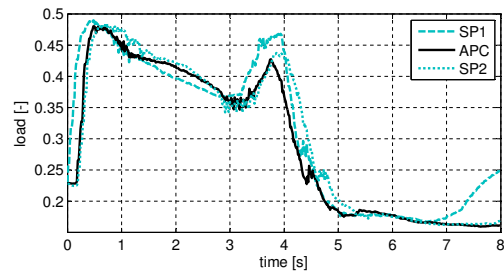
We compared the performance of the APC with a gain-scheduled Smith Predictor (SP). The SP was designed based on the plant models identified at different operating points (corresponding to different combinations of engine speeds and loads) using a relay feedback method.

Figure 12 shows the results of an acceleration-deceleration test conducted using the test vehicle. The performances are very similar as can be seen in Fig. 12a and Fig. 12d, where the time evolutions of Φ and the error integral is presented. On the other hand, Fig. 12c shows that the control signal of the APC is smoother than that of the SP.

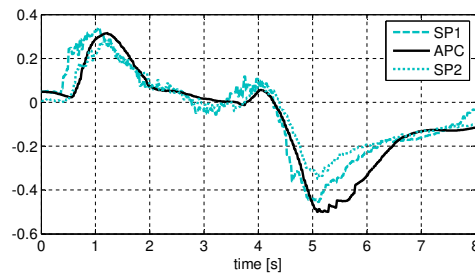
Figure 12 confirms that the adaptive controller is performing very well and similar in performance to the Smith Predictor. Note that the gain-scheduled SP can be seen as a perfect adaptive controller: While the APC *adapts* to operating point changes without the knowledge of the plant parameters, the gain-scheduled SP *uses* the knowledge of the changing plant parameters that



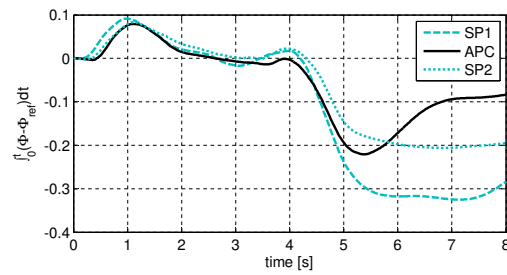
(a)



(b)



(c)



(d)

Fig. 12. Time histories of a) Φ b) Engine relative air flow c) Feedback control input d) Tracking error integral, during vehicle acceleration and deceleration for gain-scheduled SP vs. APC, with $c = 1.5$.

need to be obtained offline by using an identification procedure for different operating points. The adaptive controller can, in addition, adjust better to situations when plant parameters change due to part-to-part variability or aging. For example, it is stated in [7] that due to aging or harsh operating conditions, UEGO sensor time constant can easily increase by a factor of 10 to 20. Also it is known that the Smith Predictor is sensitive to the delay estimation errors.

In Fig. 13, we present the simulation results that compare SP with APC. For this simulation, the time constant for the first order system model is selected as 50 ms, which is reported in [7] as the time constant of a state-of-the-art oxygen sensor. The nominal time delay is assumed to be 0.4 seconds. A step input disturbance is introduced to this plant at time $t = 170$ seconds and the transients are plotted. The APC and the SP is tuned such that they perform similarly for these nominal plant parameter values, in the presence of the disturbance. Then, the sensor time constant is increased by a factor of 20 and the disturbance test is repeated. As seen in the figure, not only the performance of the SP gets worse than the adaptive controller, but the SP response also becomes oscillatory, which is a sign of getting closer to instability. An additional uncertainty in the system, like a delay identification error, may cause the system to become unstable easily. Indeed, when we introduce a delay uncertainty by increasing the nominal delay by 0.3 seconds, we see that the loop with the SP becomes almost marginally stable. This simulation result is presented in Fig 14.

V. SUMMARY

In this paper, we have considered the fuel-to-air ratio (FAR) control problem in port-fuel-injection (PFI) spark-ignition (SI) engine. Two controllers, an Adaptive FeedForward Controller (AFFC) and an Adaptive Posicast Controller (APC), have been developed and implemented in a test vehicle. The AFFC is a simple controller based on feedforward adaptation, while the APC is a more elaborate controller that uses adaptation in both feedforward and feedback paths and is based on a recently developed adaptive control method for time-delay systems. The AFFC has been shown in simulations and experiments to have better reference tracking and similar disturbance rejection capabilities when compared to the existing baseline controller. The APC has been shown in experiments to achieve faster recovery from disturbances and better performance during vehicle acceleration deceleration tests. These performance improvements were a result of various modifications and enhancements to the initial APC design, such as an algorithm to

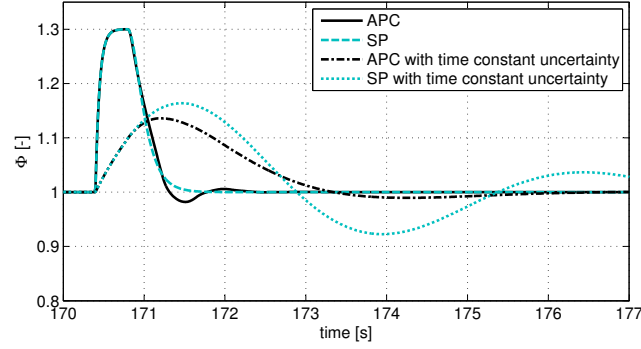


Fig. 13. Comparison of SP and APC for input step disturbance rejection in the presence of sensor time constant uncertainty.

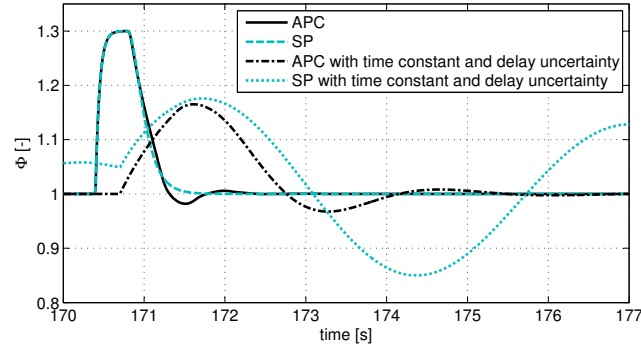


Fig. 14. Comparison of SP and APC for input step disturbance rejection in the presence of sensor time constant and delay uncertainty.

handle the variable time delay, a robustness scheme and parameter initialization and fine tuning methods. It has also been observed in our vehicle experiments that implementing APC using an upper bound on the delay as a delay estimate assures robustness against delay variations.

In terms of applications of the APC, the FAR control problem is more challenging than the Idle Speed Control (ISC) problem, which the authors of this paper have treated in [33] and [40], due to a larger and variable time delay and different character of disturbances and uncertainties. The experimental results reported here demonstrate that the APC is effective for the FAR control problem as well.

APPENDIX A

DISTURBANCE REJECTION PROOF

When there is a constant disturbance $d \in \Re$ present in the system, the state space description of the plant (12) is modified as

$$\dot{x}_p(t) = A_p x_p(t) + b_p(u(t - \tau) + d), \quad y(t) = h_p^T x_p(t) \quad (33)$$

This in turn modifies the error equation (23) as

$$\begin{aligned} \dot{e}(t) &= A_m e(t) + b_m [\tilde{\alpha}^T(t - \tau) \omega(t - \tau) \\ &\quad + \int_{-\tau}^0 \tilde{\lambda}(t - \tau, \sigma) u(t - \tau + \sigma) d\sigma \\ &\quad + \tilde{k} r(t - \tau) + d] \\ e_1(t) &= h_m^T e(t). \end{aligned} \quad (34)$$

Note that in FAR control application, the FAR reference, $r_0 \in \Re$, is constant and therefore we have $r(t - \tau) = r_0$ in (34). We define a new variable \tilde{k}' as

$$\tilde{k}' = \tilde{k} + \frac{d}{r_0} \quad (35)$$

Therefore, (34) reduces to

$$\begin{aligned} \dot{e}(t) &= A_m e(t) + b_m [\tilde{\alpha}^T(t - \tau) \omega(t - \tau) \\ &\quad + \int_{-\tau}^0 \tilde{\lambda}(t - \tau, \sigma) u(t - \tau + \sigma) d\sigma \\ &\quad + \tilde{k}' r_0] \\ e_1(t) &= h_m^T e(t). \end{aligned} \quad (36)$$

which can also be written as

$$\begin{aligned} \dot{e}(t) &= A_m e(t) + b_m [\tilde{\theta}'^T(t - \tau) \Omega(t - \tau) \\ &\quad + \int_{-\tau}^0 \tilde{\lambda}(t - \tau, \sigma) u(t - \tau + \sigma) d\sigma] \\ e_1(t) &= h_m^T e(t). \end{aligned} \quad (37)$$

where, $\tilde{\theta}' = \begin{bmatrix} \tilde{\alpha}_1 & \tilde{\alpha}_2 & \tilde{k}' \end{bmatrix}^T$. Equations (37) and (34) are exactly the same equations written using different variables, meaning that the definition of the new variable does not alter the equilibrium position of the differential equation. In addition, (37) is in the same form as in the

case of disturbance free system (24), and hence the stability proof follows along the same lines and $\lim_{t \rightarrow \infty} e_1(t) = 0$. Therefore, the system is stable, the disturbance is rejected and the plant output follows the reference model output asymptotically.

To conclude, disturbance rejection is achieved by eliminating the disturbance term in the error equation and this is done by introducing a new variable defined by shifting the feedforward controller term k by a constant.

ACKNOWLEDGMENT

This work was supported through the Ford-MIT Alliance Initiative. The authors would like to acknowledge Dr. Davor Hrovat of Ford Motor Company for his support and encouragement during this project. The authors also wish to acknowledge Steve Magner and John Michelini of Ford Motor Company for their help and valuable discussions.

REFERENCES

- [1] L. Guzzella and C. H. Onder, *Introduction to Modeling and Control Internal Combustion Engine Systems*, 1st ed. Springer, 2004.
- [2] M. Shelef and R. W. McCabe, "Twenty-five years after introduction of automotive catalysts: what next?" *Catalysis Today*, vol. 62, no. 1, pp. 35–50, Sep. 2000.
- [3] L. Guzzella, "Models and model-based control of IC-engines A nonlinear approach," *SAE Paper*, no. 950844, 1995.
- [4] B. Ault, V. K. Jones, J. D. Powell, and G. F. Franklin, "Adaptive air-fuel ratio control of a spark-ignition engine," *SAE Paper*, no. 940373, 1994.
- [5] R. Turin and H. Geering, "Model-reference adaptive A/F ratio control in an SI engine based on Kalman-Filtering techniques," in *Proc. Amer. Control Conf.*, 1995, pp. 4082–4090.
- [6] V. K. Jones, B. A. Ault, G. F. Franklin, and J. D. Powell, "Identification and air-fuel ratio control of a spark ignition engine," *IEEE Transactions on Control Systems Technology*, vol. 3, no. 1, Mar. 1995.
- [7] D. Rupp, C. Onder, and L. Guzzella, "Iterative adaptive air/fuel ratio control," in *Proc. Advances in Automotive Control*, Seascape Resort, USA, 2008.
- [8] L. Guzzella, M. Simons, and H. P. Geering, "Feedback linearizing air/fuel-ratio controller," *Control Eng. Practice*, vol. 5, no. 8, pp. 1101–1105, Aug. 1997.
- [9] C.-F. Chang, N. P. Fekete, A. Amstutz, and J. D. Powell, "Air-fuel ratio control in spark-ignition engines using estimation theory," *IEEE Transactions on Control Systems Technology*, vol. 3, no. 1, Mar. 1995.
- [10] J. D. Powell, N. P. Fekete, and C. F. Chang, "Observer-based air-fuel ratio control," *IEEE Control Systems Magazine*, vol. 18, no. 5, pp. 72–83, Oct. 1998.
- [11] S. B. Choi and J. K. Hedrick, "An observer-based controller design method for improving air/fuel characteristics of spark ignition engines," *IEEE Transactions on Control Systems Technology*, vol. 6, no. 3, pp. 325–334, May 1998.
- [12] M. Won, S. B. Choi, and J. K. Hedrick, "Air-to-fuel ratio control of spark ignition engines using gaussian network sliding control," *IEEE Transactions on Control Systems Technology*, vol. 6, no. 5, pp. 678–687, Sep. 1998.

- [13] J. K. Pieper and R. Mehrotra, "Air/fuel ratio control using sliding mode methods," in *Proc. Amer. Control Conf.*, San Diego, CA, June 1999, pp. 1027–1031.
- [14] J. S. Souder and J. K. Hedrick, "Adaptive sliding mode control of air-fuel ratio in internal combustion engines," *Int. J. Robust Nonlin. Cont.*, vol. 14, no. 6, pp. 525–541, Apr. 2004.
- [15] A. Ohata, M. Ohashi, M. Nasu, and T. Inoue, "Crank-angle domain modeling and control for idle speed," *SAE Paper*, no. 950075, 1995.
- [16] C. H. Onder and H. P. Geering, "Model-based multivariable speed and air-to-fuel ratio control of an si engine," *SAE Paper*, no. 930859, 1993.
- [17] C. W. Vigild, K. P. H. Andersen, E. Hendricks, and M. Struwe, "Towards robust H-infinity control of an SI engine's air/fuel ratio," *SAE Paper*, no. 1999-01-0854, 1999.
- [18] L. Mianzo, H. Peng, and I. Haskara, "Transient air-fuel ratio H_∞ preview control of a drive-by-wire internal combustion engine," in *Proc. Amer. Control Conf.*, 2001, pp. 2867–2871.
- [19] S. Nakagawa, K. Katogi, and M. Oosuga, "A new air-fuel ratio feedback control for ulev/sulev standard," *SAE Paper*, no. 2002-01-0194, 2002.
- [20] Y.-J. Zhai and D.-L. Yu, "Neural network model-based automotive engine air/fuel ratio control and robustness evaluation," *Engineering Applications of Artificial Intelligence*, in press.
- [21] K. R. Muske and C. P. J. Jones, "A model-based si engine air fuel ratio controller," in *Proc. Amer. Control Conf.*, 2006, pp. 3284–3289.
- [22] C. F. Chang, N. P. Fekete, and J. D. Powell, "Engine air-fuel ratio control using an event-based observer," in *Proc. of SAE*, no. 930766, 1993.
- [23] A. G. Stefanopoulou, J. W. Grizzle, and J. S. Freudenberg, "Engine air-fuel ratio and torque control using secondary throttles," in *Proc. of Conference on Decision and Control*, 1994, pp. 2748–2753.
- [24] Z. F., K. Grigoriadis, M. Franchek, and I. Makki, "Linear parameter varying lean burn air-fuel ratio control for a spark ignition engine," *Journal of Dynamic Systems, Measurement and Control*, vol. 129, pp. 404–414, 2007.
- [25] P. Tunestal and J. K. Hedrick, "Cylinder air/fuel ratio estimation using net heat release data," *Control Eng. Practice*, vol. 11, no. 3, pp. 311–318, Mar. 2003.
- [26] I. Arsie, C. Pianese, G. Rizzo, and V. Cioffi, "An adaptive estimator of fuel film dynamics in the intake port of a spark ignition engine," *Control Eng. Practice*, vol. 11, no. 3, pp. 303–309, Mar. 2003.
- [27] S.-I. Niculescu and A. M. Annaswamy, "An adaptive smith-controller for time-delay systems with relative degree $n \leq 2$," *Systems and Control Letters*, vol. 49, pp. 347–358, 2003.
- [28] Y. Yildiz, A. Annaswamy, I. Kolmanovsky, and D. Yanakiev, "Adaptive posicast controller," *Automatica*, submitted. <http://web.mit.edu/aacslab/publications/index.html>.
- [29] O. J. Smith, "A controller to overcome dead time," *ISA Journal*, vol. 6, 1959.
- [30] A. Z. Manitius and A. W. Olbrot, "Finite spectrum assignment problem for systems with delays," *IEEE Transactions on Automatic Control*, vol. 24, no. 4, 1979.
- [31] K. Ichikawa, "Frequency-domain pole assignment and exact model-matching for delay systems," *International Journal of Control*, vol. 41, pp. 1015–1024, 1985.
- [32] R. Ortega and R. Lozano, "Globally stable adaptive controller for systems with delay," *International Journal of Control*, vol. 47, no. 1, pp. 17–23, 1988.

- [33] Y. Yildiz, A. Annaswamy, D. Yanakiev, and I. Kolmanovsky, “Adaptive idle speed control for internal combustion engines,” in *Proc. Amer. Control Conf.*, New York City, July 2007, pp. 3700–3705.
- [34] —, “Adaptive air fuel ratio control for internal combustion engines,” in *Proc. Amer. Control Conf.*, Seattle, Washington, June 2008, pp. 2058–2063.
- [35] —, “Automotive powertrain control problems involving time delay: An adaptive control approach,” in *Proc. of ASME Dynamic Systems and Control Conference*, Ann Arbor, Michigan, Oct. 2008.
- [36] S. Majhi and D. P. Atherton, “Obtaining controller parameters for a new Smith predictor using autotuning,” *Automatica*, vol. 36, no. 11, pp. 1651–1658, Nov. 2000.
- [37] K. S. Narendra and A. M. Annaswamy, *Stable Adaptive Systems*. Englewood Cliffs, NJ: Prentice-Hall, 1989.
- [38] K. Engelborghs, M. Dambrine, and D. Roose, “Limitations of a class of stabilization methods for delay systems,” *IEEE Trans. Automatic Control*, vol. 46, no. 2, Feb. 2001.
- [39] S. P. Karason and A. M. Annaswamy, “Adaptive control in the presence of input constraints,” *IEEE Trans. Automatic Control*, vol. 39, no. 11, pp. 2325–2330, Nov. 1994.
- [40] Y. Yildiz, A. Annaswamy, D. Yanakiev, and I. Kolmanovsky, “Spark ignition engine idle speed control: An adaptive control approach,” *IEEE Transactions on Control Systems Technology*, submitted. <http://web.mit.edu/aacslab/publications/index.html>.
- [41] M. J. van Nieuwstadt, I. V. Kolmanovsky, P. E. Moraal, A. Stefanopoulou, and M. Jankovic, “EGR-VGT control schemes: experimental comparison for a high-speed diesel engine,” *IEEE Control Systems Magazine*, vol. 20, no. 3, pp. 63–79, Jun. 2000.



Yildiray Yildiz Biography text here.



Anuradha Annaswamy Biography text here.

PLACE
PHOTO
HERE

Diana Yanakiev Biography text here.

PLACE
PHOTO
HERE

Ilya Kolmanovsky Biography text here.